Available online at www.sciencedirect.com
ScienceDirect
Journal of Solid State Chemistry 180 (2007) 2175–2185
JOURNAL OF SOLID STATE CHEMISTRY
www.elsevier.com/locate/jssc

^{17}O NMR studies of local structure and phase evolution for materials in the $Y_2Ti_2O_7$–$ZrTiO_4$ binary system

John L. Palumbo[a], Tobias A. Schaedler[b], Luming Peng[a], Carlos G. Levi[b], Clare P. Grey[a,*]

[a]*Department of Chemistry, State University of New York, Stony Brook, NY 11794-3400, USA*
[b]*Materials Department, University of California, Santa Barbara, CA 93106-5050, USA*

Received 4 January 2007; received in revised form 25 April 2007; accepted 30 April 2007
Available online 18 May 2007

Abstract

^{17}O MAS NMR and XRD studies of precursor-derived $Y_{1.6}Zr_{0.4}Ti_2O_{7.2}$ and $Y_{1.2}Zr_{0.8}Ti_2O_{7.4}$ have been performed to investigate the development of local and long-range order in these materials as they evolve from a metastable amorphous state upon heating. Zirconium titanate ($ZrTiO_4$) was also investigated to help interpret the ^{17}O NMR spectra of the ternary compositions. Consistent with earlier studies, crystallization was observed at 800 °C to form a fluorite structure and a small amount of rutile; weak broad reflections were also observed which were ascribed to the presence of small pyrochlore-like ordered domains or particles within the fluorite phase. As the temperature was increased further, the sizes of these domains grew along with the concentration of rutile. At the highest temperature studied (1300 °C), the reflections of the thermodynamic phases, pyrochlore and zirconium titanate ($ZrTiO_4$), dominated the XRD pattern. The ^{17}O NMR spectra revealed a series of different peaks that were assigned to different 3- and 4-coordinate O local environments. The data were consistent with the formation of a metastable phase $Y_{2-x}Zr_xTi_{2-y}Zr_yO_{7+x}$ with pyrochlore-like ordering but with Zr substitution on both cation sites of the pyrochlore structure. At low temperatures, doping on the A (Y^{3+}) sites predominates (i.e., $x>y$), consistent with the fact that the pyrochlore develops out of a more disordered fluorite-like, phase. As the temperature is raised, the Zr doping on the A site decreases and the metastable phase at this temperature can now be written as $Y_{2-x'}Zr_{x'}Ti_{2-y'}Zr_{y'}O_{7+x'}$ (i.e., $x'<y'$); TiO_2 is also observed, consistent with this suggestion. At high temperatures, doping on the B site decreases and the resonances due to the stoichiometric pyrochlore yttrium titanate ($Y_2Ti_2O_7$) dominate the NMR spectra. Weaker ^{17}O NMR resonances due zirconium titanate ($ZrTiO_4$) are also observed.

Keywords: Oxygen-ion conduction; MAS NMR; Pyrochlore; Fluorite; Metastable states; Yttrium titanate; Yttrium zirconate

1. Introduction

Ternary oxides of general formula $A_2B_2O_{7+\delta}$ (with, for example, A, $B = Y^{3+}$, Ti^{4+}, Zr^{4+}), have been shown to exhibit moderate-to-good oxygen ion conductivity [1]. Applications of these and related materials range from oxygen sensors and electrodes, to electrolytes for solid oxide fuel cells (SOFCs) [2]. Many $A_2B_2O_7$ oxides adopt either the pyrochlore or fluorite structure depending on the sizes of the A and B cations, but fluorite can sometimes occur metastably in materials that form pyrochlores, if the materials are doped and/or synthesized at low homologous temperatures [3,4]. Cation doping in $Y_2Ti_2O_7$ has been studied by using techniques such as X-ray diffraction (XRD), thermo-gravimetric analysis (TGA), differential scanning calorimetry (DSC), transmission electron microscopy (TEM) and MAS NMR spectroscopy [3,5–8].

Neutron diffraction studies of the $Y_2Ti_2O_7$–$Y_2Zr_2O_7$ quasi-binary examined the pyrochlore-to-fluorite transition, as well as the relationship between cation mixing on the A and B sites and the occupancy of the vacant O3 site of the pyrochlore structure [7,8]. ^{17}O MAS NMR spectroscopy was

*Corresponding author.
E-mail addresses: jpalumbo@ic.sunysb.edu (J.L. Palumbo), tobias@engineering.ucsb.edu (T.A. Schaedler), pengluming@gmail.com (L. Peng), levic@engineering.ucsb.edu (C.G. Levi), cgrey@notes.cc.sunysb.edu (C.P. Grey).

0022-4596/$ - see front matter © 2007 Elsevier Inc. All rights reserved.
doi:10.1016/j.jssc.2007.04.027

subsequently used by Kim and Grey [5] to investigate the local structure in this binary system.

A recent study by Schaedler et al. [3] described the phase evolution of initially amorphous, precursor-derived compositions along the $Y_2Ti_2O_7$–$Y_2Zr_2O_7$ and $Y_2Ti_2O_7$–$Zr_2Ti_2O_8$ ($ZrTiO_4$) tie lines. The approach involved heat-treating samples of the amorphous mixed oxides at different temperatures and characterizing the transformation products with XRD, TEM and DSC [3]. Pyrochlore, fluorite, $ZrTiO_4$ and rutile phases were all observed depending on the starting composition and the heat treatment used during synthesis, the results providing insight into the metastable phase evolution in the $YO_{1.5}$–TiO_2–ZrO_2 system. This current paper reports results from an ^{17}O MAS NMR study of local structure for two compositions of general formula $Y_{2-x}Zr_xTi_2O_{7+x}$, where $x = 0.2$ (10 mole% ZrO_2, denoted 10Zr) and 0.4 (20Zr), in the $Y_2Ti_2O_7$–$Zr_2Ti_2O_8$ tie line. Amorphous samples of these compositions were prepared by sol–gel routes and heated at various temperatures in order to follow the changes in local structure in the metastable phases that occur upon heat treatment, and to relate the changes in local structure to the long-range structural rearrangements.

1.1. Structures

The pyrochlore structure (space group $Fd\bar{3}m$), adopted by the end-member $Y_2Ti_2O_7$, is derived from the fluorite structure, but the cations, ($A^{3+} = Y^{3+}$) and ($B^{4+} = Ti^{4+}$), are ordered on two different crystallographic sites (Fig. 1a) resulting in a doubling of the cell parameters over those of fluorite. This cation ordering results in three different possible sites for oxygen O1 (1/8, 1/8, 1/8; Wyckoff position 8*a*), O2 (x, 1/8, 1/8; 48*f*) and O3 (3/8, 3/8, 3/8; 8*b*). These oxygen sites are all four coordinated, but are associated with distinct anion coordination environments O2A_4, O1A_2B_2 and O3B_4. Here, and throughout the paper, the notation $OM_xM'_y$ indicates that the oxygen anion is coordinated to xM^{n+} and $yM'^{n'+}$ cations in its first coordination shell. The O3 site is not occupied in a stoichiometric pyrochlore such as $Y_2Ti_2O_7$, but may sometimes be partially occupied on cation doping (e.g., in $Y_2Ti_{2-x}Zr_xO_7$) [4,6,8]. In the more disordered fluorite structure ($Fm\bar{3}m$ space group), adopted by for example $Y_2Zr_2O_7$, the oxygen atoms are similarly tetrahedrally coordinated, but a range of local environments $OA_{4-x}B_x$ will be present.

The structure of the material with nominal composition $ZrTiO_4$ is more complex, since the ordering and stoichiometry of this compound are strongly affected by pressure, the presence of other metal cation dopants, and thermal history. $ZrTiO_4$ has a structural phase transition at just below 1200 °C. The high-temperature form of $ZrTiO_4$ belongs to space group *Pbcm* [9] and adopts the α-PbO_2 structure, wherein the cations are completely disordered over one crystallographic site. The Zr:Ti ratio in this phase is not fixed, the possible deviations from the ideal 1:1

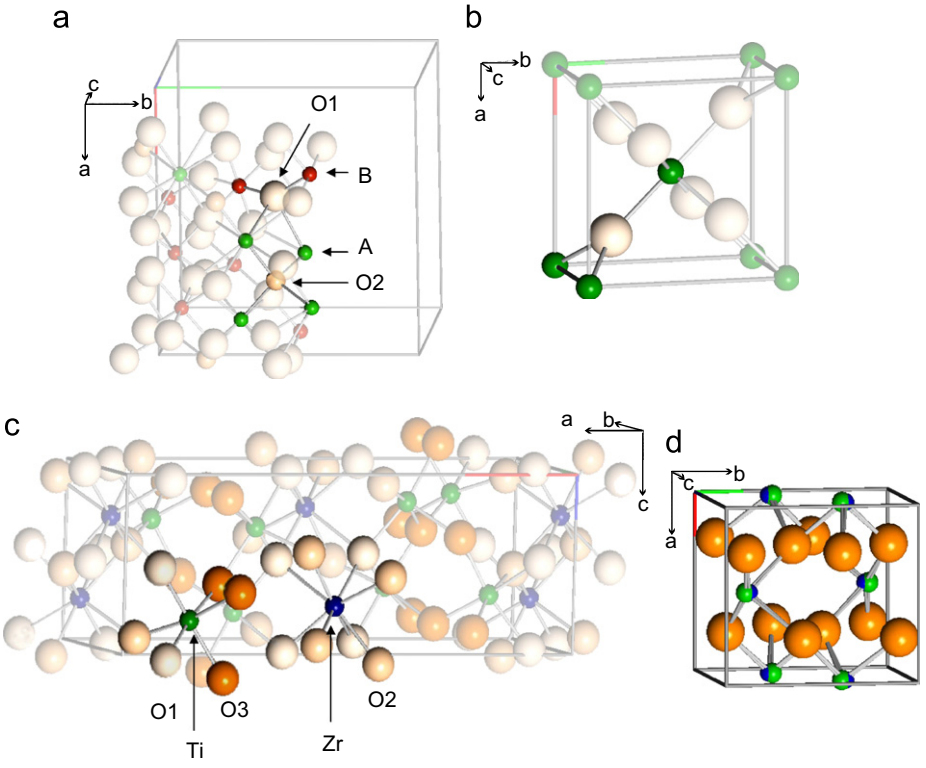

Fig. 1. (a) Pyrochlore structure showing the two local oxygen environments O1A_2B_2 and O2A_4. (b) Room temperature structure of rutile. The local OTi_3 environment is shown along with the unit cell (Ti small spheres, oxygen large sphere). (c) The unit cell of the partially ordered $Zr_5Ti_7O_{24}$ structure; the 6-coordinate Ti and 8-coordinate Zr are highlighted. (d) The high-temperature (α-PbO_2) structure of $ZrTiO_4$.

stoichiometry, increasing as the temperature is raised above the phase transition [10]. α-PbO_2 is structurally related to fluorite, the ions shifting to form distorted, edge-sharing MO_6 octahedra [11] which form a zigzag pattern along the *c*-axis (Fig. 1b) [12]. The cations order below 1200 °C, the extent of ordering depending on the cooling rate from the disordered state, and any cation doping. The cation ordering results in the formation of alternating double slabs with Ti–Ti–Zr–Zr–Ti–Ti–Zr–Zr sequences along the *c*-direction [9]. A Zr-deficient material $Zr_5Ti_7O_{24}$ is similarly derived from the α-PbO_2 structure, with almost complete ordering to form alternating single Zr and double Ti-rich slabs Ti–Ti–Zr–Ti–Ti–Zr [10]. High-resolution TEM studies of ordered materials close to the nominal $ZrTiO_4$ composition, showed that Ti–Ti–Zr- and Ti–Ti–Zr–Zr-blocks can coexist, the single slabs existing as uniformly distributed faults within the structure, and resulting in regions with Zr:Ti ratios of less than 1 [9]. A recent, ambient temperature phase diagram for the ZrO_2–TiO_2 binary reported by Troitzsch et al. [10] reveals even more complexity and explains why exsolution of TiO_2 and baddeleyite can sometimes be seen on rapid cooling [13]. An ordered phase with a close to 1:1 stoichiometry is stable between approximately 1160 and 1080 °C, while below this temperature, the ordered phase with a composition close to that of $Zr_5Ti_7O_{24}$ (in equilibrium with Ti^{4+}-doped ZrO_2) represents the thermodynamic phase.

1.2. Local structure and NMR spectroscopy

To aid in the interpretation of the NMR spectra of these materials, the local environments present in these phases need to be considered. The neutron diffraction results for $Zr_5Ti_7O_{24}$ showed that the oxygen atoms of the ordered phase remain 3-coordinate in between the Ti–Ti slabs, but a displacement of the oxygen environments in between the Ti and Zr slabs occurs so that the OTi_2Zr local environment is coordinated to a fourth Zr at a slightly longer distance, forming an OTi_2Zr_2 environment (Fig. 1c) and 8-coordinate Zr ions. Although no neutron diffraction data are available for any partially ordered (metastable) $ZrTiO_4$ materials, it seems likely that similar displacements of the oxygen atoms may occur, if domains containing Zr slabs are present, similarly resulting in $O(M,M')_4$ environments, in addition to the $O(M,M')_3$ environments found in the disordered α-PbO_2 phase. However, a relatively recent Zr and Ti EXAFS study of the crystallization of phases with this composition, below the order–disorder transition, did not show any evidence for the formation of Zr coordination environments of higher than 6 [14].

The ^{17}O MAS NMR spectra of some of the phases relevant to this investigation have been reported [5], the results demonstrating that the ^{17}O chemical shift of the different local environments in these solids depends strongly on both the oxygen coordination number and the nature of the directly bound cations. The pyrochlore $Y_2Ti_2O_7$ contains two distinct, sharp resonances at 457 and 385 ppm, which are assigned to the two tetrahedrally coordinated oxygen sites $O2Y_4$ and $O1Y_2Ti_2$, with associated multiplicities of 1:6 (O1:O2). Rutile has a single ^{17}O NMR resonance with a reported shift of 588 ppm [15], corresponding to the trigonally coordinated O local environment OTi_3 (see Fig. 1b). The ^{17}O NMR spectrum of $ZrTiO_4$ has yet to be reported. Possible impurities in $ZrTiO_4$ are monoclinic ZrO_2 (Baddeleyite), which contains 3- and 4-coordinate local environments with associated ^{17}O NMR resonances at 401 and 324 ppm, respectively [15], and tetragonal ZrO_2, which contains a single OZr_4 local environment which resonates at 376 ppm. The results are consistent with the general observation that oxygen atoms in lower coordination environments resonate at higher frequencies [5,16,17].

The introduction of dopants on the cation sites can create different local environments for oxygen, despite the oxygen occupying the same crystallographic site in the lattice. If these environments occur randomly within the sample, these will not be directly visible by XRD. For example, the ^{17}O NMR spectrum of the fluorite $Y_2Zr_2O_7$ contains a very broad resonance centered at about 360 ppm, which corresponds to the single crystallographic site of fluorite [5]. The broadening arises from the presence of different local environments, OY_xZr_{4-x}, in this compound each with slightly different chemical shifts. In the 10Zr and 20Zr compounds, there are several possible local oxygen environments that should, in principle, resemble local environments in related structures. The chemical shifts of the various relevant local environments were estimated in our previous ^{17}O study on pyrochlores [5]. Based on these results, it is clear that a substitution for Ti by Zr (or Y) in the local environments $OTi_{3-x}Y_x$ (or $OTi_{3-x}Zr_x$) will result in an approximately additive shift in the ^{17}O NMR resonance to lower frequency, by approximately 36 ppm per Y^{3+} substitution (and slightly more for Zr^{4+} substitution) for the pyrochlore materials. The results are summarized in Table 1, in order to help in the subsequent interpretation of the NMR data.

Table 1
Summary of the ^{17}O shifts of different O local environments from references [15,5]

Local environment	Oti_3		OY_2Ti_2	OY_4	OY_2Zr_2	OZr_4		OZr_3
Material	Rutile	Anatase	$Y_2Ti_2O_7$	$Y_2Ti_2O_7$	$Y_2Zr_2O_7$	*t*-ZrO_2	*m*-ZrO_2	*m*-ZrO_2
Shift (referenced to H_2 ^{17}O, ppm)	588[15]	557[15]	457[5]	385[5]	360[5]	376[15]	324[15]	401[15]

Table 2
Heat treatment and ^{17}O enrichment technique for the studied compounds

Compound stoichiometry	Label	Heat treatment (C) in air	^{17}O enrichment technique (24 h)
10Zr	10Zr 800	800/1 h	Evacuated pyrex tube, 550 °C
	10Zr 1000	1000/5 h	Evacuated pyrex tube, 550 °C
	10Zr 1300	1300/5 h	Evacuated pyrex tube, 1000 °C
20Zr	20Zr 800	800/1 h	Evacuated pyrex tube, 550 °C
	20Zr 1000	1000/5 h	Evacuated pyrex tube, 550 °C
	20Zr 1300	1300/5 h	Evacuated pyrex tube, 550 °C
$ZrTiO_4$	ZT 700	700/1 h	
	ZT 1000		Evacuated pyrex tube, 1000 °C

In this work, XRD and ^{17}O MAS NMR were used to examine both long-range structure and the local environments surrounding the oxygen atoms for the two compositions: 10 and 20Zr. ^{17}O MAS NMR spectra of rutile and $ZrTiO_4$ are first presented to help the subsequent analysis of the local order that arises in the first coordination sphere of oxygen in the two compounds under investigation, 10Zr ($Y_{1.6}Zr_{0.4}Ti_2O_7$) and 20Zr ($Y_{1.2}Zr_{0.8}Ti_2O_7$). The results from these studies are described in the context of the earlier study by Schaedler et al. [3].

2. Experimental

The syntheses of $Y_{1.2}Zr_{0.8}Ti_2O_7$ (20Zr), $Y_{1.6}Zr_{0.4}Ti_2O_7$ (10Zr) and $ZrTiO_4$ (ZT) are identical to those described earlier [3]. A reverse co-precipitation method was used, with precursors yttrium nitrate, titanium *iso*-propoxide and zirconium *n*-butoxide, mixed in *iso*-propanol (HPLC grade) in stoichiometric amounts. The resultant solution was added drop-wise to aqueous ammonium hydroxide at a constant pH of 10. The pH was maintained by simultaneous addition of NH_4OH. The resultant precipitates were filtered, dried, ground using a mortar and pestle and pyrolyzed at 700 °C for 1 h at 10 °C/min. Heat treatments (summarized in Tables 2 and 3) were performed by preheating the furnace and placing the samples, contained in open alumina crucibles in the furnace at 800 °C/1 h, 1000 °C/5 h and 1300 °C/5 h. These samples are labeled with the following notation 10Zr 800, indicating that the 10Zr sample was heated at 800 °C. The 10Zr, 20Zr and ZT samples, as well as a sample of rutile TiO_2 (Alfa Aesar, 99.99% purity [catalogue #14631]), were then enriched with $^{17}O_2$ gas (50% concentration $^{17}O_2$, Isotec) by heating the samples at 550–600 °C for 24 h in a sealed Pyrex vacuum tube. A second set of samples was prepared by heating the pyrolyzed sample in a sealed quartz tube with enriched $^{17}O_2$ gas. The sealed quartz ampoule was placed in a room temperature furnace and heated to 1000 °C over 5 h then allowed to cool to room temperature. The $ZrTiO_4$ precursor was first heated for 1 h at 700 °C to induce crystallization, and subsequently enriched with $^{17}O_2$ gas in a sealed quartz tube by heating to 1000 °C overnight. The heat-treatment and $^{17}O_2$-enrichment protocols for all the samples are listed in Table 2. A Rigaku Miniflex XRD bench top X-ray diffractometer was used to assure sample purity both before and after enrichment for all samples.

Table 3
Phases seen from XRD

	$^{17}O_2$ enrichment	10Zr	20Zr
800 (°C)	Before	f? + P (5 nm) + r(vw)	f? + P + r(w)
	After (550 °C)	f? + P (30 nm) + r(vw)	f? + P + r(w)
1000 (°C)	Before	P (10 nm) + r	P (11 nm) + r + z
	After (550 °C)	P (47 nm) + r	P (34 nm) + r + z
1300 (°C)	Before	P (24 nm) + r(w) + z (vw)	P (>60 nm) + r(w) + z
	After (1000 °C)	P (>60 nm) + r(w) + z (vw)	P (>60 nm) + r(w) + z

Average particle sizes are calculated for the pyrochlore phase (in parentheses) using the Debye–Scherrer formula. At 1300 °C, the line widths of the reflections are governed by the instrumental resolution (f: fluorite, P: pyrochlore, r: rutile, z: $ZrTiO_4$, vw: very weak, w: weak).

^{17}O MAS NMR experiments were performed with a double or triple resonance 4 mm MAS Chemagnetics probes on either an Infinity Plus 360 or 500 MHz spectrometer operating at 48.8 or 67.7 MHz, respectively, with a rotor spinning speed of 15 kHz. One pulse and Hahn echo ($\pi/2$–τ–π–τ) pulse sequences were used with solid $\pi/2$ pulses of 1.3 μs. The ^{17}O reference was $H_2^{17}O$ (10% ^{17}O, Isotec.) which was set to 0 ppm. Spectral deconvolution was performed with the NUTS software.

3. Results

3.1. Model compounds

The spectrum of rutile is dominated by a single isotropic resonance at 589 ppm with a line width of ~720 Hz, which is assigned to the OTi_3 local environment shown in Fig. 1a, consistent with the shift reported in earlier studies (588 ppm) [15].

XRD revealed that the $ZrTiO_4$ amorphous precursor had crystallized upon heat treatment at 700 °C/1 h, in agreement with our earlier report [3] and other sol–gel

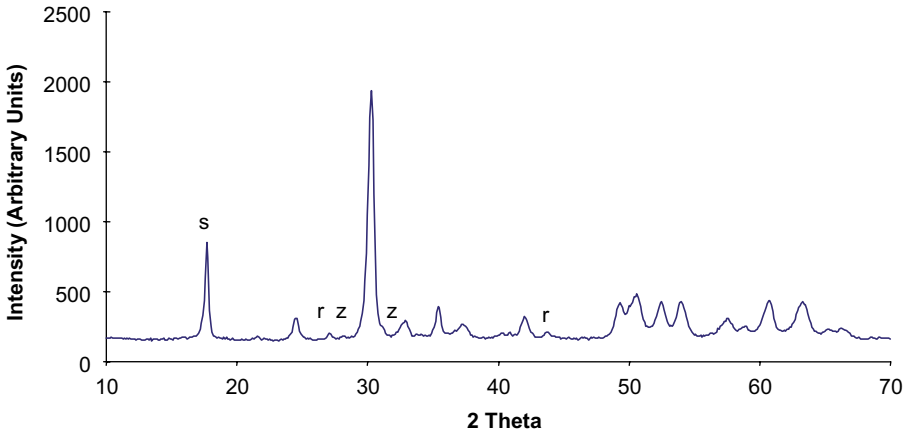

Fig. 2. XRD pattern of $ZrTiO_4$ post $^{17}O_2$ gas enrichment at 1000 °C. Rutile and monoclinic ZrO_2 are indicated as R and Z, respectively, and the sample holder as S.

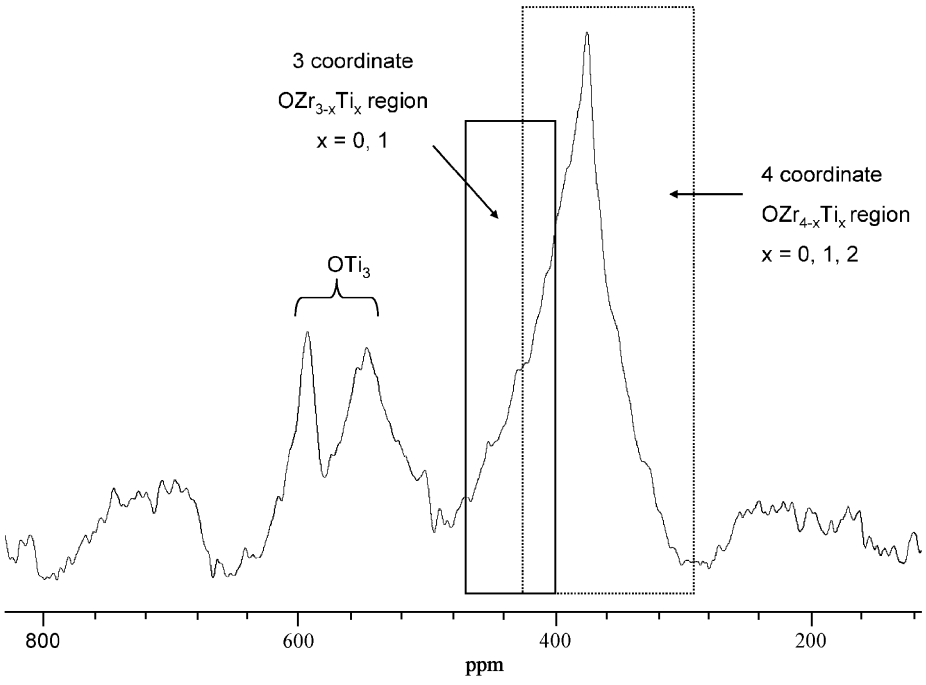

Fig. 3. ^{17}O MAS NMR 1 pulse spectrum of ZT 1000 collected at 8.45 T.

studies of this composition [14]. The XRD pattern for the sample heated at 700 °C/1 h and then at 1000 °C/5 h (ZT1000; Fig. 2) shows reflections due to $ZrTiO_4$ and small amounts of rutile and baddeleyite (monoclinic ZrO_2) second phases, consistent with earlier observations [13]. A sharp resonance is observed in the ^{17}O MAS NMR spectrum of ZT1000 (Fig. 3) at approximately 594 ppm, which is close to the isotropic resonance of rutile, and is therefore assigned to the OTi_3 local environment in the excess rutile phase. The resonance at 564 ppm is assigned to a second OTi_3 oxygen environment, which is present in the Ti-rich double layers in ordered $Zr_5Ti_7O_{24}$ and is likely to be present at least to some degree in $ZrTiO_4$ prepared at 1000 °C which may show local ordering. The average OM_3 ($M = Zr$, Ti) environment in the high temperature form of $ZrTiO_4$ has a different local geometry than in rutile, presumably accounting for the slightly different chemical shift for this environment. The O–Ti–O bond angles in rutile (Fig. 1b) are $90° \times 4$, $98° \times 2$ and $81° \times 2$ where the O_3Ti are in a trigonal planar arrangement [18], whereas the O–Ti–O bond angles in $ZrTiO_4$ range between 83° and 102° and the O_3Ti group is no longer planar. The Ti is displaced slightly out of the plane formed by the three oxygen atoms lowering the symmetry [19], increasing the distortion of the local environment of oxygen. The increased breadth of resonance relative to that from rutile is ascribed to a range of distortions for the OTi_3 local environment.

All the other 3- and 4-coordinate local environments in ZT1000 must be contained within the broad envelope that spreads from approximately 460 to 320 ppm. The maximum of this broad resonance (374 ppm) occurs at the same chemical shift as the OZr_4 environment in *t*-ZrO_2 but at higher frequency than the same environment in *m*-ZrO_2 (Table 1). Resonances at frequencies of $\leqslant$374 ppm are therefore consistent with environments such as OZr_3Ti and OZr_4, which are predicted to resonate at approximately 360 and 324 ppm, respectively, based on the shifts seen for *m*-ZrO_2 [15] and those for the pyrochlores and fluorites listed in Table 1. Since both Ti-for-Zr substitution in the O coordination sphere, and a lower coordinate environment result in a shift to positive frequencies (Table 1), components of the lineshape at even higher frequencies are ascribed to increased Ti substitution and/or to lower O coordination environments. Not all the (theoretically) possible local environments (e.g., OTi_2Zr, $OTiZr_2$, OZr_3, OZr_3Ti, OZr_2Ti_2, $OZrTi_3$) are present. High concentrations of Ti-rich or low coordinate environments such as $OZrTi_3$ and $OZrTi_2$ can be excluded, which are expected to resonate at $>$450 and approximately 500 ppm, respectively (assuming additive shifts for these local environments). Interestingly, this is consistent with the structure of $Zr_5Ti_7O_{24}$, where the structural distortion transforms the OZr_2Ti environment into an OZr_2Ti_2 environment.

3.2. Heat treatment of 10Zr

The long-range structures of $Y_{1.6}Zr_{0.4}Ti_2O_{7.2}$ observed following different heat treatments, as detected by XRD (Fig. 4), are given in Table 3, while the NMR spectra are shown in Fig. 5. The XRD patterns reveal that the amorphous phase has crystallized by 800 °C and that the fluorite and rutile structures are clearly present at this temperature (Fig. 5). The broader reflection at 39° corresponds to the 331 reflection of the pyrochlore structure and suggests that some cation ordering has already occurred at this stage. Based on the full-width at half-maximum (FWHM) line width of this reflection, the average size of the pyrochlore domains is estimated to be approximately 5 nm. The size of the domains grows slightly on annealing at 550 °C in $^{17}O_2$. At 1000 °C, the pyrochlore and rutile phases are clearly visible by XRD and NMR, and the size of the pyrochlore domains has grown to ~10 nm (47 nm after annealing in $^{17}O_2$). The results suggest that the coherence length scale of pyrochlore-like ordering increases with annealing time. The unit cell parameters were extracted from the reflections common to both the pyrochlore and fluorite phases and vary from 10.06, 10.12, to 10.08 Å for 10Zr 800, 1000 and 1300, respectively. Following heat treatment at 1300 °C, the sample is dominated by the pyrochlore phase but also contains weak reflections due to $ZrTiO_4$ and very weak reflections due to rutile.

The NMR spectra of the 10Zr series in Fig. 5 are in qualitative agreement with the XRD data. Starting with the spectrum that easiest to interpret, i.e., that of 10Zr 1300, two dominant resonances are observed at 454 and 385 ppm which are assigned to the $O1Y_2Ti_2$ and $O2Y_4$ local environments respectively of the pyrochlore structure in Fig. 1a [5]. Neither of these resonances can be fit by a single Lorentzian or Gaussian lineshape and both show evidence of broader components in their baselines indicating some

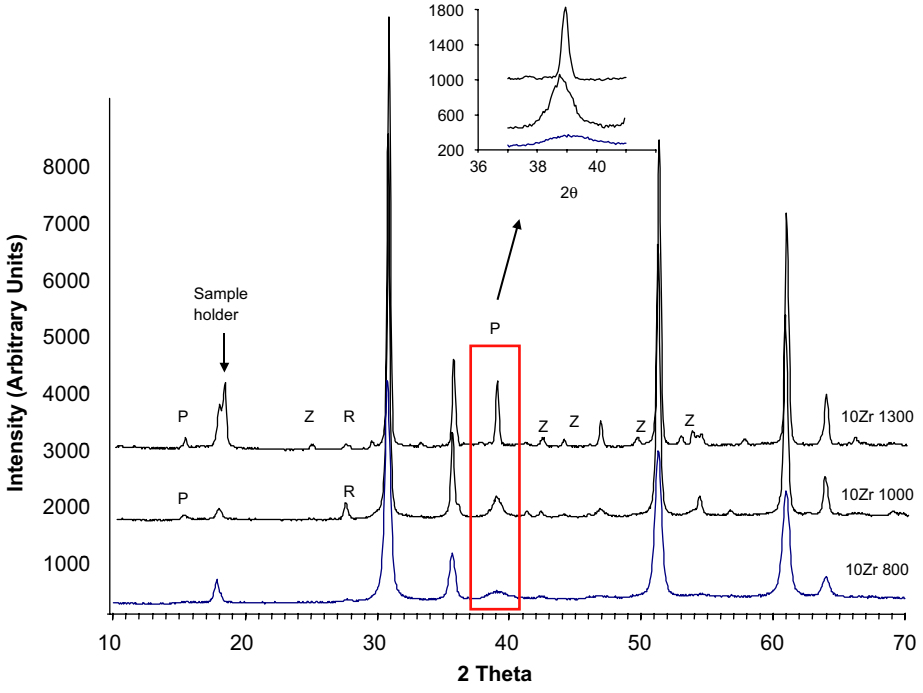

Fig. 4. XRD of the 10Zr series. Inlay shows the evolution of the pyrochlore peaks (P: pyrochlore, R: rutile, Z: $ZrTiO_4$).

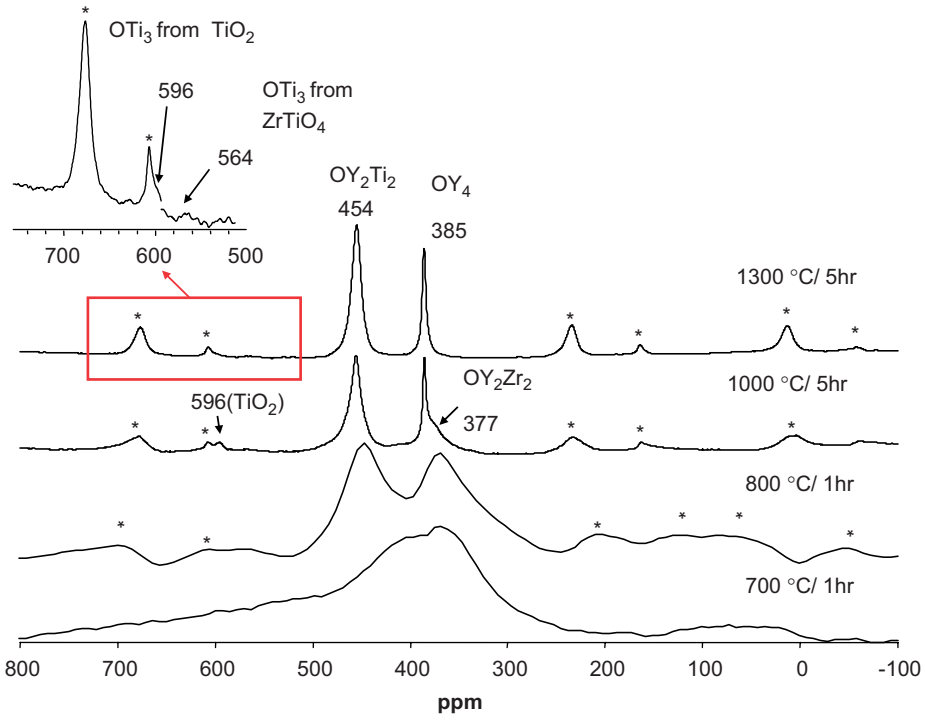

Fig. 5. ^{17}O MAS NMR 1 pulse spectra of $Y_{1.6}Zr_{0.4}Ti_2O_{7.2}$ (10Zr series) from amorphous, 800, 1000, and 1300 °C shown (from bottom to top), collected at 11.6 T. Asterisks indicate spinning sidebands.

residual disorder in the pyrochlore phase. The inset to the spectrum of 10Zr_1300 shows an enlargement of the higher frequency region where weak characteristic resonances due to TiO_2 and $ZrTiO_4$ are observed.

At 1000 °C, the pyrochlore (455 and 385 ppm) and rutile (596 ppm) phases are clearly visible by NMR and XRD (Figs. 5 and 4). A broader resonance at approximately 377 ppm is also observed in the NMR spectra, along with a weaker broad resonance at 411 ppm; these can be seen more clearly in Fig. 6. Earlier work by Kim et al. suggests that substitution of Y^{3+} by Zr^{4+} in the oxygen local coordination sphere of environments $OY_{4-x}Zr_x$ in Zr^{4+}-doped $Y_2Ti_2O_7$ results in small ^{17}O NMR shifts to lower frequencies of approximately 7–10 ppm per Zr^{4+} for Y^{3+} replacement. Much larger shifts to higher frequency are expected when Ti^{4+} substitutes for Y^{3+} in the O local coordination shell. Since the new resonance at 411 ppm lies intermediate between the $O2Y_4$ and $O1Y_2Ti_2$ resonances (Table 1), we tentatively ascribe it to $OY_{3-x}Zr_xTi$, i.e., a 4-coordinate O resonance, most likely in the pyrochlore phase, containing only one Ti^{4+} in its local coordination sphere and 3 Y^{3+}/Zr^{4+} ions. The lower frequency resonance at 377 ppm is very close in chemical shift to both the main resonance seen in $ZrTiO_4$ in the sample prepared under similar temperature conditions and the $OZrY_3$ environment in a pyrochlore (approximately 373 ppm). A weak, broader resonance is also observed at 564 ppm, which is likely associated with the OTi_3 environment in $ZrTiO_4$, indicating that local environments in this phase must also contribute to the intensity of the 377 ppm resonance. Presumably, the sizes of the crystallites are too small to allow the $ZrTiO_4$ phase to be detected by XRD at this temperature. A weaker resonance due the OTi_3 environments of rutile is seen at 596 ppm. Deconvolution of resonances found in the spectral region from 550 to 300 ppm suggests that there may also be additional very broad resonances to lower frequencies of the main pyrochlore peaks, at approximately 450 and 360 ppm. These resonances are present in the 10Zr 800 (Fig. 5) spectrum with much higher intensities and are tentatively assigned to environments such as OY_2Ti_2 (450 ppm) and OY_2Zr_2 and OY_3Zr in the 360 ppm region.

Two resonances dominate the spectrum of 10Zr 800 (Fig. 5) with chemical shifts close to those found for $Y_2Ti_2O_7$, although the two sets of resonances are much broader and have shifted to lower frequencies (447 and 368 ppm, Fig. 7). Again, the resonance at 368 ppm is assigned to Ti-free local environments such as OY_3Zr and OY_2Zr_2; these environments have very similar shifts (approximately 373 and 360 ppm [5]) and it is therefore difficult to resolve them. Deconvolution of the lineshape (Fig. 7) suggests that at least one more resonance at even lower frequencies (approximately 322 ppm) is required to reproduce the lineshape. Based on the shift for the 4-coordinate environment in monoclinic-ZrO_2 at 324 ppm [15], this resonance is assigned to the OZr_4 local environment. The much weaker resonance at 412 ppm is assigned to $OY_{3-x}Zr_xTi$.

The ^{17}O NMR spectrum of the amorphous material (Fig. 5) is dominated by two overlapping resonances at approximately 420 and 370 ppm, which are tentatively assigned to $OY_{3-x}Zr_xTi$ and OY_2Zr_2, respectively.

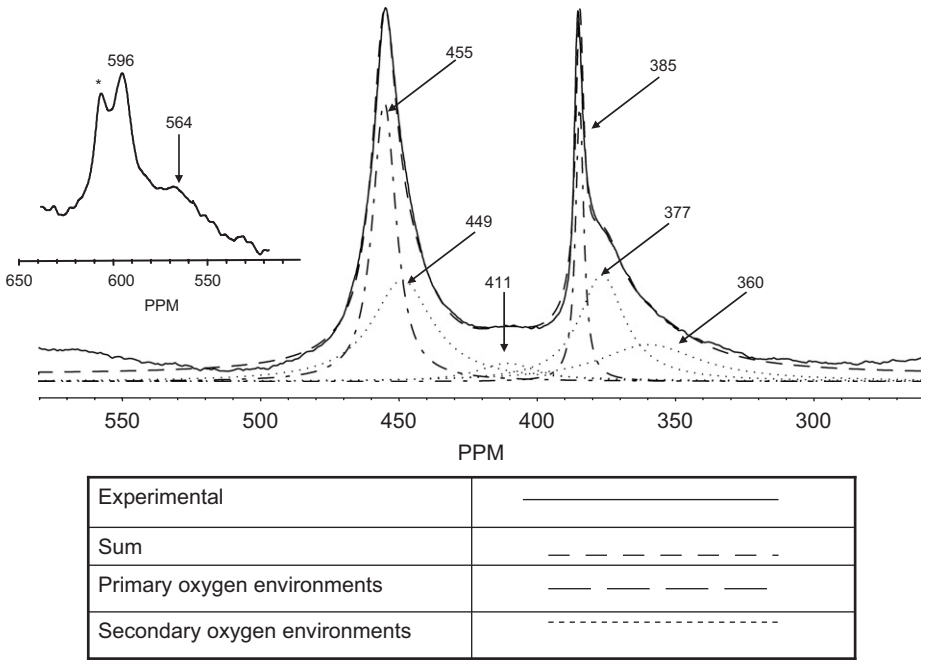

Fig. 6. Deconvolution of the two main ^{17}O NMR resonances of the 10Zr 1000 spectrum showing the contribution of the different oxygen local environments to the spectrum. An expansion of the higher frequency region is shown in an inset.

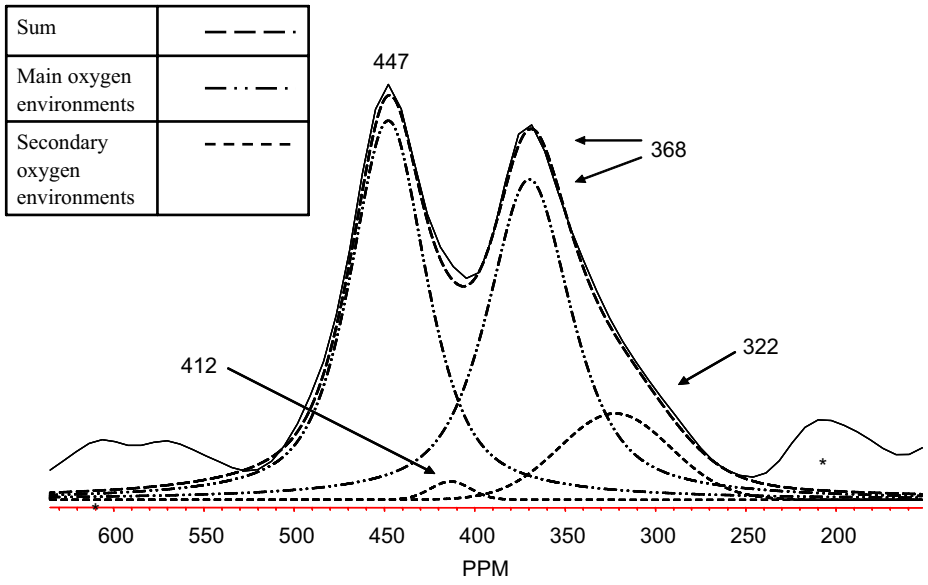

Fig. 7. Deconvolution of the 10Zr 800 spectrum showing two main oxygen environments and two secondary environments.

Both these resonance are broad, suggesting that other Ti-deficient local environments (e.g., OY_3Zr and $OYZr_3$) are present. A very broad resonance to higher frequency is observed which is ascribed to the Ti-rich environments (e.g., OTi_3 or OTi_2Zr/Y).

3.3. Heat treatment of 20Zr

The phases seen by XRD for the $Y_{1.2}Zr_{0.8}Ti_2O_{7.4}$ composition are similar to those seen for 10Zr at the three temperatures studied (800 °C/1 h, 1000 °C/5 h, 1300 °C/5 h) (Fig. 8; Table 3). However, the pyrochlore phase is relatively less well developed at 800 and 1000 °C, and the reflections due to $ZrTiO_4$ are more intense at 1300 °C, consistent with the higher concentration of Zr in this sample. Weak reflections due to *t*-ZrO_2 are also observed at 1000 °C. The ^{17}O NMR spectra of the $Y_{1.2}Zr_{0.8}Ti_2O_{7.4}$ series are shown in Fig. 9. All three data sets contain similar isotropic resonances as the 10Zr spectra; however, there are some noticeable differences. The resonances in all three spectra of the 20Zr series are broader, relative to the 10Zr series. The signal-to-noise (S/N) of these spectra is

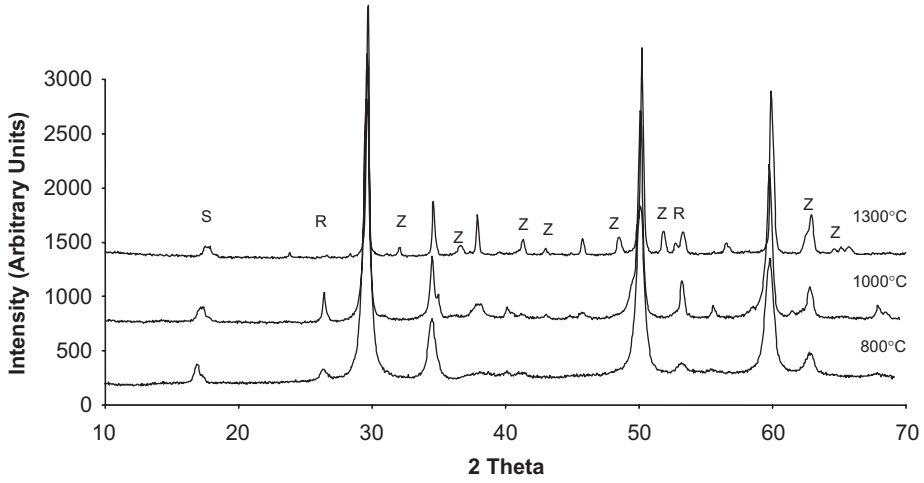

Fig. 8. XRD patterns of the 20Zr series. S: sample holder, R: rutile, Z: $ZrTiO_4$.

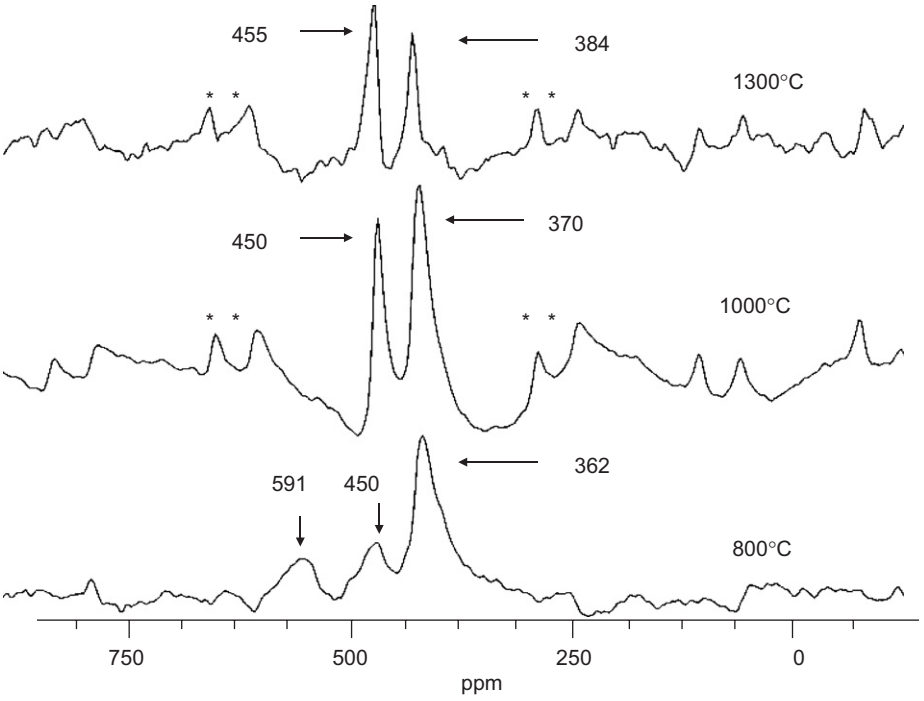

Fig. 9. ^{17}O MAS NMR spectra collected at 8.45T for the 20Zr series ($Y_{1.2}Zr_{0.8}Ti_2O_{7.4}$); top to botom, heat treatment at 1300, 1000 and 800 °C. Asterisks indicate first order spinning sidebands

also worse than those for 10Zr, in part due to the broader resonances. For the sample annealed at 1300 °C, the poorer S/N is also ascribed to the different enrichment method (see Table 2). Other causes of the decrease in S/N include different sample volumes used in the enrichment process, oxygen-leaks in the enrichment system and poorer oxygen-mobility in the higher Zr containing samples (leading to difficulties in enrichment). The spectrum of the material at 800 °C exhibits three main isotropic resonances at 591 ppm (OTi_3), 450 ppm ($OYZrTi_2$) and 362 ppm (OY_3Zr and OY_2Zr_2). At 1000 °C, the lowest frequency resonance has shifted to 370 ppm, and subsequently to 384 ppm at 1300 °C. This is consistent with a decrease in the Zr concentration in the local coordination shell, with 384 ppm corresponding to the $O2Y_4$ local environment. The resonance due to *t*-ZrO_2 (Table 1) in the spectrum of 20Zr1000 is presumably contained in the 370 ppm resonance. The S/N of these spectra are too poor to allow the $ZrTiO_4$ and TiO_2 resonances to be identified unambiguously at higher temperatures.

4. Discussion

The evolution of the long-range structures was summarized in Table 2; the implications from NMR concerning the doping of the cations within these phases and the extent of

ordering will now be explored. Not until 10Zr and 20Zr are heated to ~800 °C for an hour are crystalline structures observed by diffraction and well resolved resonances seen in the NMR spectra. The observation of small pyrochlore domains by diffraction (approximately 5 and 30 nm, before and after ^{17}O enrichment), and the similarity of the ^{17}O NMR spectrum to that of the ordered pyrochlore phase seen at higher temperature, suggest that small domains of pyrochlore-like ordering are present at 800 °C and above. Sharp peaks are present for the reflections that are characteristic to both the fluorite and pyrochlore phases indicating that peak broadening is not a consequence of small particle sizes, and that on a longer length-scale, the lattice is fluorite-like. The 10Zr spectrum is dominated by two resonances that are assigned to the local environments $OZrYTi_2$ and OY_2Zr_2. Given the pyrochlore-like ordering, these resonances must originate from the O1 ($O1A_2B_2$) and O2 ($O2A_4$) sites, in the pyrochlore structure. Only a very weak resonance due to the O2 local environment OY_2TiZr (411 ppm) is observed in the spectrum of 10Zr 800, which would arise from substitution of the B site by Zr. This indicates that Zr predominantly substitutes for Y on the A site of the pyrochlore structure, in the small pyrochlore domains that are present at low temperature. This forms a metastable phase with composition $(Y_{2-x}Zr_x)(Ti_{2-y}Zr_y)O_{7+x}$ $(x>y)$. The 20Zr spectra are also consistent with this hypothesis, since the $OZrYTi_2$ and OY_2Zr_2 resonances are similarly observed at this temperature. As the material is heated further to 1000 °C, the environment $OY_{3-x}Zr_xTi$ is now observed clearly for 10Zr (the S/N of 20Zr spectrum is not good enough to allow more detailed analysis). This indicates that the Zr ions have now substituted for Ti in the B site to form $Y_2Ti_{2-y'}Zr_{y'}O_7$, either due to movement of Zr ions from the A to the B site, (some) Zr remaining in the structure, or preferential removal of Zr from the A sites and, thus, from the structure. The former proposal will be accompanied by Ti removal from the pyrochlore domains; this is consistent with the observation of rutile by both NMR and XRD in higher concentrations. The latter proposal is supported by the emergence of a tetragonal zirconia phase in the XRD patterns of some samples of 20Zr, heated at intermediate temperatures (1100 °C) [20], suggesting that both mechanisms occur for the 20Zr sample. In 10Zr, the smaller Zr concentrations of Zr ions can probably be accommodated by moving them from the A to B sites (preferred by Zr^{4+} due to its valence and size), which is accompanied by Ti removal from the B sites, consistent with the appearance of a rutile phase. As the temperature is increased to 1300 °C, more Zr is rejected from the structure and phases such as $ZrTiO_4$ are seen more clearly by XRD, although this phase was detected at 1000 °C by NMR for 10Zr.

The variations in occupancies of the different ions in the different sites of the pyrochlore structure are consistent with the lattice parameters of the phases (derived from the full set of reflections from pyrochlore and fluorite). The smallest lattice parameter (1.006 nm) is estimated observed for 10Zr_800 ($Y_{2-x}Zr_xTi_{2-y}Zr_yO_{7+x}$ $(x>y)$), consistent with the substitution of the smaller Zr^{4+} ion (ionic radius 0.206 nm) for Y^{3+} (0.212 nm) on the Y^{3+} site. As Zr^{4+} is removed from this site, forming $Y_2Ti_{2-y'}Zr_{y'}O_7$, the lattice parameter increases to 1.012 nm, due to both substitution of Zr^{4+} for the much smaller Ti^{4+} ion on the B site (and the accompanying elimination of Ti^{4+} from the structure), and the removal of Zr^{4+} from the A site. Assuming no residual substitution of Zr on the A site, a lattice parameter of 1.012 is consistent with a value for y of approximately 0.2 [7]. Finally, the lattice parameter drops again to 10.08 Å, as the Zr^{4+} concentration on the pyrochlore B site decreases and $ZrTiO_4$ is precipitated. A similar trend was observed for 20Zr. Interestingly, the unit cell parameters derived for the pyrochlore superstructure reflections are similar (within error) to those estimated for the whole set of fluorite + pyrochlore reflections (1.004 ($\pm$0.002) nm, 1.010 ($\pm$0.002) for 1.007 ($\pm$0.001) for 800, 1000 and 1300Zr, respectively. This further implies that the pyrochlore is ordering out of a fluorite phase rather than being present as a separate, distinct phase. The NMR spectrum of the amorphous phase (10Zr 700) suggests that Ti-rich and Ti-poor local environments are present, indicating that Y and Zr-rich fluorite like domains may even be starting to form in the nominally amorphous material, along with regions more rich in Ti. This may explain why the pyrochlore phase that crystallizes at low temperatures contains Zr doping on the Y (A) site. However, it is important to stress that our NMR experiments are only probing structure in the first cation coordination shell, so it is not possible to determine the extent of any compositional variations in the amorphous phase.

5. Conclusions

A combination of XRD and solid state NMR spectroscopy has been used to investigate the crystallization of samples with compositions $Y_{1.6}Zr_{0.4}Ti_2O_7$ and $Y_{1.2}Zr_{0.8}Ti_2O_7$. The results provide insight into the phase evolution (from the amorphous to crystalline state) observed in this system, which involves the formation of a series of metastable phases that differ in their extent of incorporation of Zr on the A and B sites of the pyrochlore $Y_2Ti_2O_7$. The results are summarized in Fig. 10. The first crystalline phase observed in this study has reflections that can by indexed as fluorite. Superstructure reflections are seen due to a metastable pyrochlore phase $Y_{2-x}Zr_xTi_{2-y}Zr_yO_{7+x}$, with a small domain size, which is derived from the stoichiometric pyrochlore $Y_2Ti_2O_7$, with Zr doping on the A (Y) and B (Ti) sites of the structure. At low temperatures, doping on the A sites predominates (i.e., $x>y$), consistent with the fact that the pyrochlore develops out of a more disordered Zr and Y-rich fluorite-like precursor phase. As the temperature is raised, Zr is exsolved from the pyrochlore, primarily from the A site. The metastable phase at this temperature can now be written as $Y_{2-x'}Zr_{x'}Ti_{2-y'}Zr_{y'}O_{7+x'}$ (i.e., $x'<y'$); TiO_2 is also observed, consistent with this suggestion. This is in

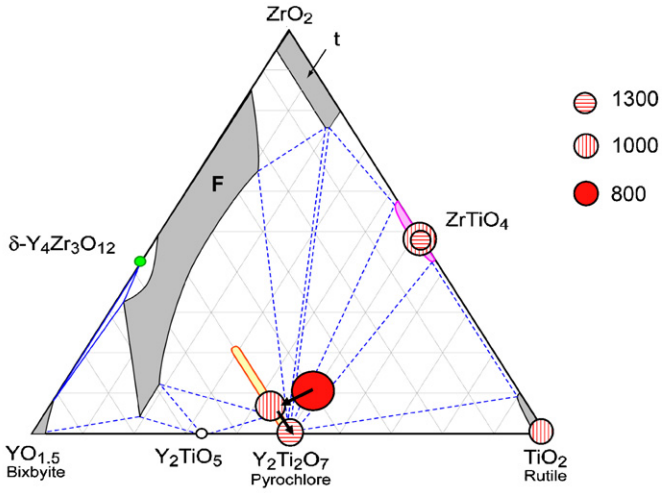

Fig. 10. Schematic of the evolution of the crystalline phases in a material with stoichiometry $Y_{1.6}Zr_{0.4}Ti_2O_{7.2}$ (10Zr), as a function of heat treatment at 800, 1000 and 1300 °C.

agreement with studies of the $Y_2Ti_2O_7$–$Y_2Zr_2O_7$ tie line where the thermodynamically stable form of the Zr-doped pyrochlore phase $Y_2(Zr_zTi_{2-z})O_7$ can accommodate Zr up to $z \leqslant 0.8$; the metastable phase in this tie line can tolerate even higher Zr dopings [3,4,6]. At high temperatures, essentially all the Zr is exsolved and the final thermodynamically stable phases, $ZrTiO_4 + Y_2Ti_2O_7$ are observed.

The paper clearly shows that the long-range probe of structure, XRD, can be combined with ^{17}O NMR to examine subtle changes in doping and in local ordering.

Acknowledgments

We thank the NSF for support of this work via the MRSEC grant DMR-0080021 and further awards to CPG (DMR 0506120 and CHE 0321001). Helpful discussions with Profs. Sanjay Sampath and John Parise are gratefully acknowledged.

References

[1] J.A. Kilner, R.J. Brook, Solid State Ion. 6 (3) (1982) 237–252.
[2] J.C. Boivin, G. Mairesse, Chem. Mater. 10 (1998) 2870–2888.
[3] T.A. Schaedler, W. Francillon, A.S. Gandhi, C.P. Grey, S. Sampath, C.G. Levi, Acta Mater. 53 (2005) 2957–2968.
[4] C. Heremans, B.J. Wuensch, J. Solid State Chem. 117 (1995) 108–121.
[5] N. Kim, C.P. Grey, J. Solid State Chem. 175 (2003) 110–115.
[6] B.J. Wuensch, K.W. Eberman, C. Heremans, E.M. Ku, P. Onnerud, E.M.E. Yeo, S.M. Haile, J.K. Stalick, J.D. Jorgensen, Solid State Ion. 129 (2000) 111–133.
[7] Y. Liu, R.L. Withers, L. Noren, J. Solid State Chem. 177 (2004) 4404.
[8] B.J. Wuensch, K.W. Eberman, C. Heremans, E.M. Ku, P. Onnerud, E.M.E. Yeo, S.M. Haile, J.K. Stalick, J.D. Jorgensen, Solid State Ion. 129 (2000) 111–133.
[9] P.K. Davies, R. Christofferson, J. Am. Ceram. Soc. 75 (3) (1992) 563–569.
[10] U. Troitzsch, A.G. Christy, D.J. Ellis, Phys. Chem. Miner. 32 (2005) 504–514.
[11] R.W. Lynch, B. Morosin, J. Am. Ceram. Soc. 55 (8) (1972) 409–413.
[12] P. Bordet, A. McHale, A. Santoro, R.S. Roth, J. Solid State Chem. 64 (1986) 30–46.
[13] U. Troitzsch, A.G. Christy, D.J. Ellis, J. Am. Ceram. Soc. 87 (11) (2004) 2058–2063.
[14] J. Xu, C. Lind, A.P. Wilkinson, S. Pattanaik, Chem. Mater. 12 (2000) 3347–3355.
[15] T.J. Bastow, S.N. Stuart, Chem. Phys. 143 (1990) 459–467.
[16] P.J. Dirken, T.J. Bastow, E. Smith, H.J. Whitfield, J. Phys. Chem. 100 (1996) 18539–18545.
[17] M.E. Smith, T.J. Bastow, H.J. Whitfield, J. Mater. Chem. 2 (9) (1992) 989–990.
[18] E.P. Meagher, G.A. Lager, Can. Min. 17 (1979) 77–85.
[19] R.E. Newnham, J. Am. Ceram. Soc. 50 (1967) 216.
[20] T. A. Schaedler, Ph.D. Thesis, U. C. Santa Barbara, 2006.